PAPER

Check for updates

The contribution of Eu³⁺ doping concentration on the modulation of morphology and luminescence properties of InVO₄:Eu³⁺

Yinyan Li [ID] and Shiqing Xu*

Nanostructures of InVO₄ and InVO₄:Eu³⁺ were synthesized through a hydrothermal method with a post annealing process. The morphology and luminescence properties of InVO₄:xEu³⁺ can be modulated by Eu³⁺ ion doping concentration. SEM and (HR)TEM studies indicated that different sizes of nanoparticles were obtained when the Eu³⁺ ion concentration ranged from 2 mol% to 30 mol%, and middle-concave nanodisks or nanoparticles with different sizes were obtained with the Eu³⁺ ion concentration ranging from 35 mol% to 45 mol%. Luminescence property studies indicated that the photoluminescence emission originated both from VO₄³⁻ and Eu³⁺, and the emission of VO₄³⁻ was blue shifted, affected by the doped Eu³⁺ ions. The CIE chromaticity diagram of Eu³⁺-doped indium vanadate exhibited green, blue-green, red, giving especially white light emission.

1 Introduction

Nowadays, materials on the mesoscopic scale are being paid more and more attention.[1] Nano-size materials with uniform morphology usually have different special characteristics, such as their magnetism, optics, conductivity and so on, due to small size effects and the specific effect of large surface area.[2,3] As we all know, InVO₄ is a semiconductor with a narrow band gap. The photoluminescence properties of InVO₄ have previously been studied.[4] Since the morphology of nanomaterials may have some important effects on their optical properties,[5] it is important to investigate various morphologies of InVO₄ in detail to obtain outstanding luminescent nanomaterials. However, nano-size InVO₄ has been rarely investigated.[6,7] Ai *et al.* synthesized nanocrystalline InVO₄ hollow microspheres with an aerosol flow synthetic method,[6] and other nano-sized indium vanadates have been synthesized by the sol–gel method and hydrothermal processes.[7] In spite of these methods for synthesis of indium vanadate nano-/micro-materials, the size distribution and regularity of these materials can still be improved. The diversity of regular and dispersed nanostructures for indium vanadates still needs to be expanded to meet their desired potential applications.

In addition, white-LEDs have attracted much attention in recent decades because of their properties of high brightness, long fluorescence lifetimes and environmental friendliness.[8] Lanthanide ions are usually codoped with each other or with transition metals in a host lattice to obtain white light

materials.[9] It is very important to find a suitable host for lanthanide luminescent centers to give white emission. In this work, we found that different emission colors including white light could be achieved from different concentrations of Eu³⁺-doped InVO₄ nanomaterials. First, Eu³⁺-doped indium vanadates were synthesized through a hydrothermal process with sodium citrate as a coordination agent. Nanostructures of the as-obtained InVO₄:xEu³⁺ with different europium ion doping concentrations were investigated. The morphology and size of the nano-indium vanadates varied regularly with the variation of the Eu³⁺ doping concentration. Different sizes of nanoparticles, middle-concave nanoparticles and middle-concave nanodisks of InVO₄:Eu³⁺ were obtained. Second, the photoluminescence properties of InVO₄:Eu³⁺ were studied to reveal the different emission spectra with different Eu³⁺ doping concentration. The CIE chromaticity diagram of Eu³⁺-doped indium vanadate exhibited green, blue-green, red, giving especially white light emission, making this material a suitable candidate for optical LEDs.

2 Experimental section

2.1 Characterization

X-ray diffraction (XRD) patterns were collected on an X-ray diffractometer (Bruker Axs D2 PHASER diffractometer) with Cu Kα radiation ($\lambda = 1.5405$ Å). SEM images were recorded on a scanning electron microscope (SEM, JSM-5601). TEM images were recorded on a transmission electron microscope (TEM JSM 2100). The photoluminescence spectra were recorded on a PL3-211-P spectrometer (HORIBA Jobin Yvon, America) and a 450W xenon lamp was used as the excitation source. The

College of Materials Science and Engineering, China Jiliang University, Hangzhou 310018, China. E-mail: sxucjlu@163.com; Fax: +86 571 28889527; Tel: +86 571 86835781

luminescence quantum efficiency (Φ) was obtained by using $BaSO_4$ as a reference.

2.2 Synthesis

General method for synthesis of $InVO_4$: 10 mL 0.1 mol L^{-1} NH_4VO_3 aqueous solution was introduced dropwise to a vigorously stirred 10 mL aqueous solution of 1 mmol $In(NO_3)_3 \cdot 5H_2O$. After addition, the mixture was stirred for 10 min, and a certain amount of sodium citrate was added to the suspension. The as-obtained yellow colloidal precipitate was transferred to a 50 mL autoclave, sealed, and heated at 150 °C for 15 h. After completion of the reaction time, the autoclave was then cooled to room temperature naturally. The products were washed three times with distilled water and centrifuged for 3 min at 10 000 rpm. The washed powders were dried under vacuum at 60 °C. The final products were obtained by annealing at 900 °C in air for 6 h and used for further investigation. For different doping concentrations in $InVO_4$:$x$$Eu^{3+}$, the same method was used with starting materials containing different proportions of $In(NO_3)_3 \cdot 5H_2O$ and $Eu(NO_3)_3 \cdot 6H_2O$.

3 Results and discussion

3.1 Synthesis and structure

The nanostructures of indium vanadate or Eu^{3+}-doped indium vanadate were synthesized by a hydrothermal method with a post annealing process. Indium(III) nitrate hydrate and ammonium vanadate were used as starting materials with sodium citrate as a complexing agent. The sodium citrate played an important role in the formation of the indium vanadate nanostructures. Control experiments without sodium citrate were carried out and irregularly shaped particles were obtained.

Fig. 1 shows the XRD patterns of the annealed hydrothermal products of $InVO_4$ and $InVO_4$ doped with various concentrations of Eu^{3+}. It indicates that the XRD of $InVO_4$ shown in Fig. 1a can be easily indexed to orthorhombic $InVO_4$ JCPDS: 71-1689. As the Eu^{3+} doping concentration increased, the XRD patterns

showed a slight change to indicate Eu^{3+} was well-doped in the crystal lattices of $InVO_4$, whose special obvious peaks are illustrated in Fig. 1. For lower doping concentrations, no obvious differences were found in the XRD patterns. When the doping-concentration of Eu^{3+} ions is higher than 10 mol% (Fig. 1b–d) the $InVO_4$ phase still remains, but the full width at half maximum of these peaks broadens.

The morphologies of $InVO_4$ and $InVO_4$:Eu^{3+} were characterized by SEM and (HR)TEM. The results indicated that uniform and dispersed nanostructures were obtained through this method. The SEM micrograph of as-obtained $InVO_4$ is shown in Fig. 2a. Regular nanoparticles with a diameter around 200 nm were formed. Fig. 3 shows the (HR)TEM and EDX results of as-obtained $InVO_4$. The TEM image of $InVO_4$ shown in Fig. 3a displays the same uniform nanoparticles as those in the SEM image (Fig. 2a). The HRTEM image (Fig. 3b) of the nanoparticles shows lattice fringes with interplanar spacing of 0.271 nm that corresponds to the (1 1 2) plane of the orthorhombic crystal structure of $InVO_4$. The EDX in Fig. 3c clearly showed the composition of the $InVO_4$ nanoparticles.

Fig. 2b–g show the SEM images of the $InVO_4$ host doped with 2, 5, 10, 15, 20 and 30 mol% of Eu^{3+} ions. They are all uniform and dispersed nanoparticles. It is obvious that as the Eu^{3+} ion concentration increased from 2 mol% to 30 mol%, the $InVO_4$:Eu^{3+} particle sizes decreased. The diameters of the
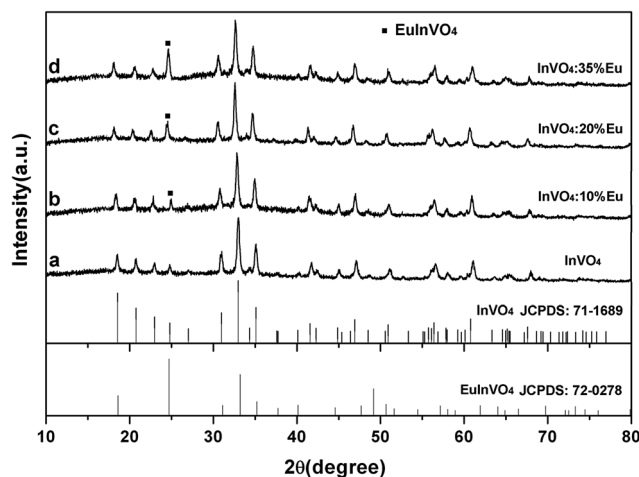

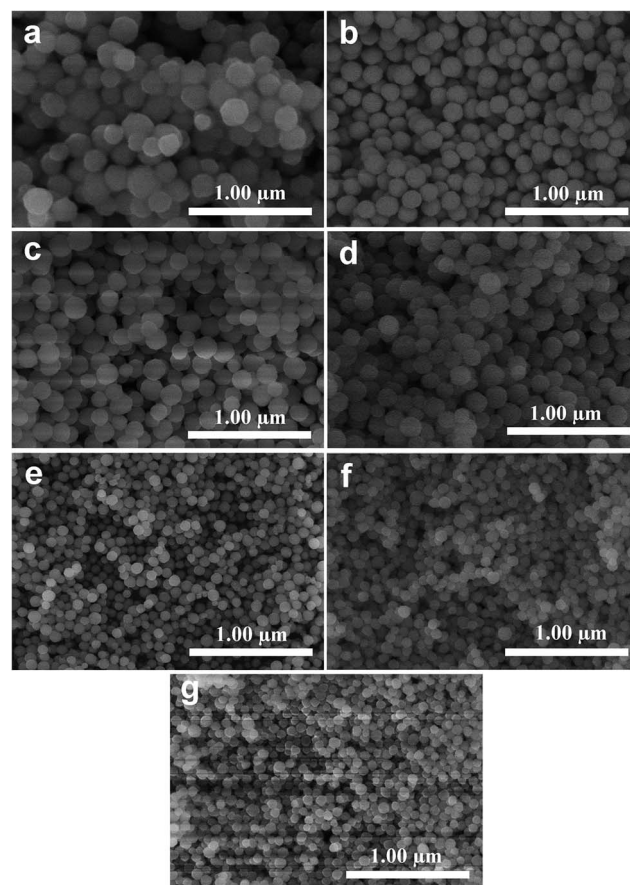**Fig. 2** SEM images of $InVO_4$ (a) and $InVO_4$:$x$$Eu^{3+}$: 2 mol% (b); 5 mol% (c); 10 mol% (d); 15 mol% (e); 20 mol% (f); 30 mol% (g).
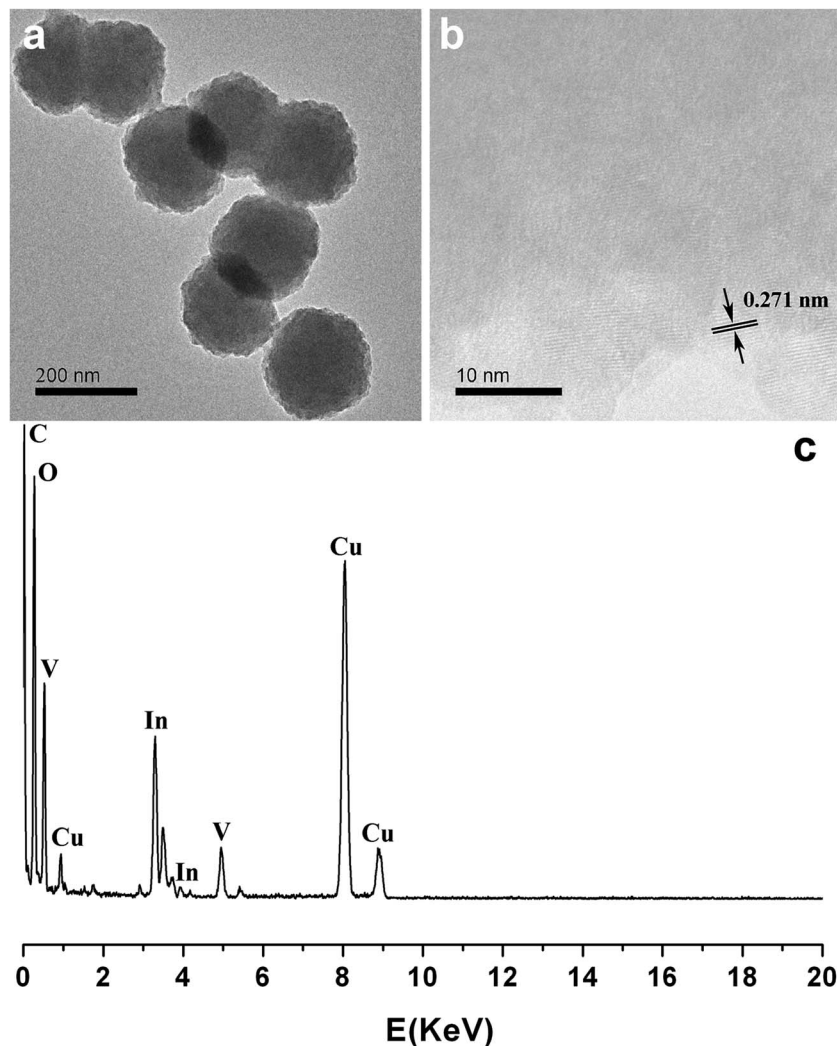

Fig. 1 XRD patterns for $InVO_4$ and $InVO_4$:Eu^{3+}.

Fig. 3 TEM (a), HRTEM (b) and EDX (c) images of InVO$_4$.

nanoparticles with different Eu^{3+} ion concentrations are given in Table 1. Diameters of the particles decreased from 200 to 50 nm with increased Eu^{3+} ion concentration. This nanoparticle diameter trend can be attributed to the large difference in the ion radius between indium(III) ions and europium(III) ions,

which is 0.8 Å for In^{3+} and 0.947 Å for Eu^{3+}.[10] The nanoparticle sizes were proven to be influenced by the nucleation and growth rates in the formation process of the nanostructures.[5] The presence of large ion radius Eu^{3+} lowered the potential barrier for the formation of nuclei and slowed the growth rates which resulted in a decrease in nanoparticle size. This is in good accordance with the nanoparticle diameter trend seen in the SEM results. In addition, slight aggregation of the calcined nano-InVO$_4$ can also be observed (Fig. 2a), while the increased doping of Eu^{3+} ions made it better and more dispersed nano-particles were obtained in Fig. 2b–g.

Fig. 4 and 5 show the SEM and TEM images of the InVO$_4$ host doped with 35, 40 and 45 mol% of Eu^{3+} ions. It is observed that when the Eu^{3+} ion doping concentrations are higher than 35 mol%, the images of the InVO$_4$:Eu^{3+} do not show nano-particles any more. Both their size and morphology changed. The morphologies and diameters of the nanostructures with different Eu^{3+} ion concentrations are collected in Table 1. InVO$_4$:35% Eu^{3+} displays special nanodisks with diameters around 180 nm. Fig. 4a and b show the SEM and TEM images of

Table 1 Morphologies and diameters of InVO$_4$ (a) and InVO$_4$: xEu^{3+}: 10 mol% (b); 20 mol% (c); 35 mol% (d)

Compounds	Morphology	Size/diameter (nm)
InVO$_4$	Nanoparticle	200
InVO$_4$:2% Eu^{3+}	Nanoparticle	180
InVO$_4$:5% Eu^{3+}	Nanoparticle	160
InVO$_4$:10% Eu^{3+}	Nanoparticle	130
InVO$_4$:15% Eu^{3+}	Nanoparticle	100
InVO$_4$:20% Eu^{3+}	Nanoparticle	70
InVO$_4$:30% Eu^{3+}	Nanoparticle	50
InVO$_4$:35% Eu^{3+}	Nanodisk	180
InVO$_4$:40% Eu^{3+}	Middle-concave particle	230
InVO$_4$:45% Eu^{3+}	Middle-concave particle	260

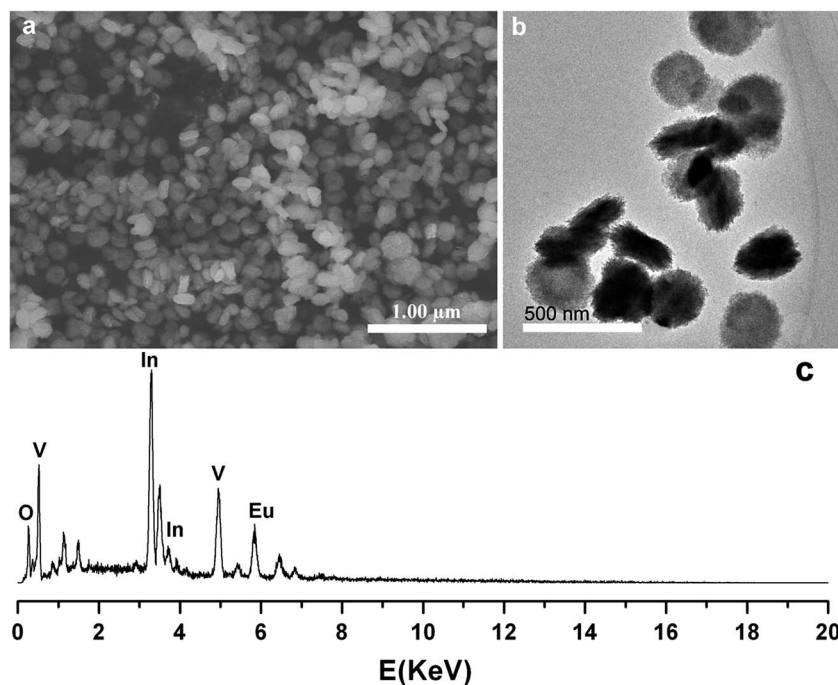**Fig. 4** SEM (a), TEM (b) images and EDX (c) of $InVO_4$:35% Eu^{3+}.

the $InVO_4$:35% Eu^{3+} nanodisks, respectively. With careful observation we can find that these nanodisks are middle-concave, and the thickness of the edge of a nanodisk is about 50 nm. The morphologies of $InVO_4$ doped with 40 mol% (Fig. 5a and b) and 45 mol% Eu^{3+} (Fig. 5c and d) are novel middle-concave nanoparticles with diameters of 230 nm for 40 mol% Eu^{3+} and 260 nm 45 mol% Eu^{3+}. The EDX shown in Fig. 4c clearly indicated the composition of the $InVO_4$: Eu^{3+} nanoparticles.

Generally, the growth process of nanocrystals includes two main steps: an initial nucleating stage and a crystal growth stage. In the first stage, the formation of seeds is crucial for further growth of the crystals (second stage). The morphologies of the final crystals are usually determined by the very early seed formation. So when the doping concentration of Eu^{3+} is lower than 30 mol%, In^{3+} dominated the initial stage of the crystal growth and different sizes of nanoparticles were obtained (as shown in Fig. 2b–g). When the doping concentration of Eu^{3+} is higher than 35 mol%, the Eu^{3+} probably had such a huge
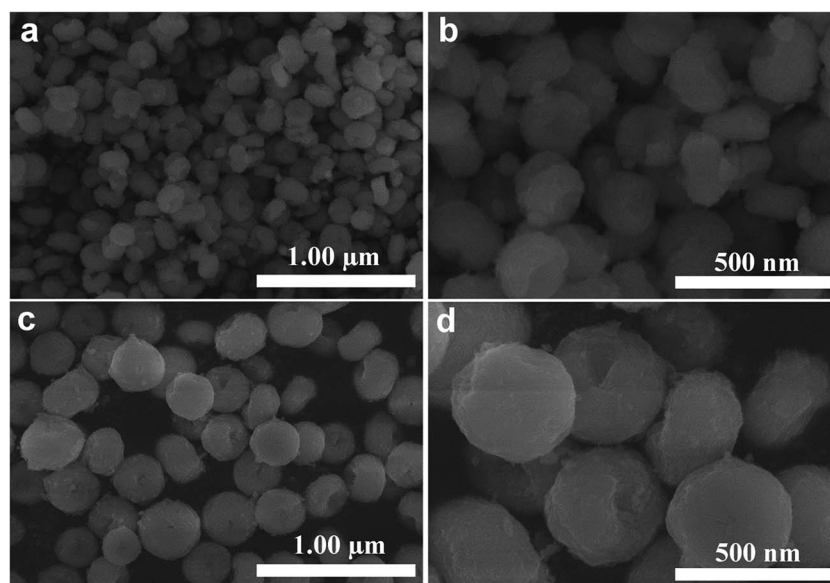

Fig. 5 SEM images of $InVO_4$:40% Eu^{3+} (a and b) and $InVO_4$:45% Eu^{3+} (c and d).
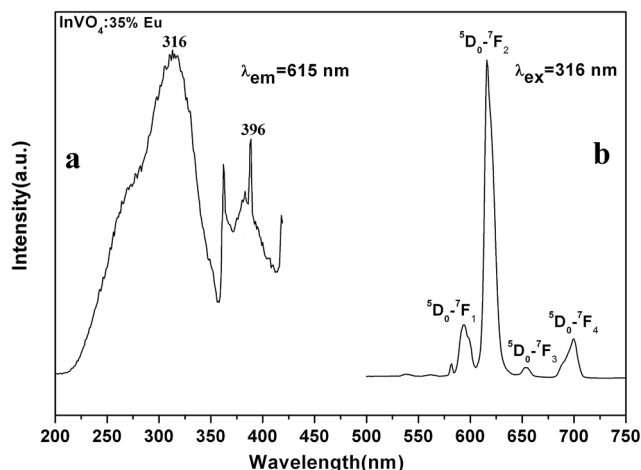
Fig. 6   Photoluminescence spectra and illustration of InVO$_4$:30% Eu^{3+}.

impact on the initial stage that the morphology of the final crystals turned out to be middle-concave nanodisks or nanoparticles. As mentioned before, the ion radius of Eu^{3+} is much bigger than that of In^{3+}, so the first nucleation stage would be changed by a higher doping concentration of bigger Eu^{3+} ions even under the same experimental conditions. So it is understandable that InVO$_4$ with Eu^{3+} doping concentrations higher than 35 mol% shows different morphologies. At the same time, we should notice that when the Eu^{3+} doping concentration is higher than 35 mol%, the sizes of the nanostructures increase with the Eu^{3+} doping concentration increasing. This is opposite to the Eu^{3+} lower doping concentration, where nanoparticle size decreased with Eu^{3+} concentration increasing (Fig. 2b–g). From the comparison of Fig. 4 and 5, we can see that InVO$_4$ with a doping concentration of Eu^{3+} from 35 mol% to 45 mol% displays middle-concave nanostructures, and the size of the nanostructures increases from 180 nm to 260 nm. From this point we can speculate that the higher Eu^{3+} doping concentrations (more than 35 mol%) in InVO$_4$ have an effect on both

morphology and size of the nanostructures. When Eu^{3+} doping concentration is higher than 50%, no regular nanostructures were obtained.

3.2   Optical properties

The room temperature photoluminescence excitation and emission spectra of InVO$_4$:30% Eu^{3+} are shown in Fig. 6. The excitation spectrum of InVO$_4$:30% Eu^{3+} monitored at 615 nm (Fig. 6a) exhibits an intense wide band centered at 316 nm, which is attributed to the charge transfer from the oxygen atoms to the central vanadium atom inside the VO$_4^{3-}$ anionic group.[11] There are several groups of sharp peaks between 360 and 400 nm which belong to the Eu^{3+} intra-4f transitions. The emission spectrum monitored at 316 nm (Fig. 6b) includes different lines of $^5D_0 \rightarrow {}^7F_J$ ($J = 1, 2, 3, 4$) multiplet transitions, in which the very strong lines ($^5D_0 \rightarrow {}^7F_2$) of hypersensitive transitions at 615 nm dominate the spectrum. Different transitions corresponding to the excitation and emission peaks are also illustrated in Fig. 6b. They are the typical well-known Eu^{3+} ion emission,[12] which will not be discussed in detail. The comparison of the emission spectra of different Eu^{3+}-doped InVO$_4$ is the important issue that needs to be noticed here. Fig. 7a depicts the photoluminescence emission spectrum of InVO$_4$ doped with different Eu^{3+} ion concentrations monitored at 316 nm. As we all know, InVO$_4$ is a self-activating phosphor.[11] When Eu^{3+} is lower than 2 mol%, the spectra are dominated by InVO$_4$ emission at 524 nm, which originates from the VO$_4^{3-}$ charge transfer transition.[13] The nanoparticles exhibited a blue-green emission under short UV irradiation. Meanwhile, in InVO$_4$:5% Eu^{3+} and InVO$_4$:8% Eu^{3+} emission spectra, the InVO$_4$ emission peak in 524 nm is reduced and a new peak at 434 nm appears, and at the same time the Eu^{3+} emission enhances. So these two nanomaterials, especially InVO$_4$:8% Eu^{3+}, display obvious white light emission. The change of the InVO$_4$:Eu^{3+} emission indicated that the Eu^{3+} was well doped in the InVO$_4$ host. The increasing doping concentration of Eu^{3+} made the emission of InVO$_4$ blue shift gradually (from 524 nm to 434 nm)
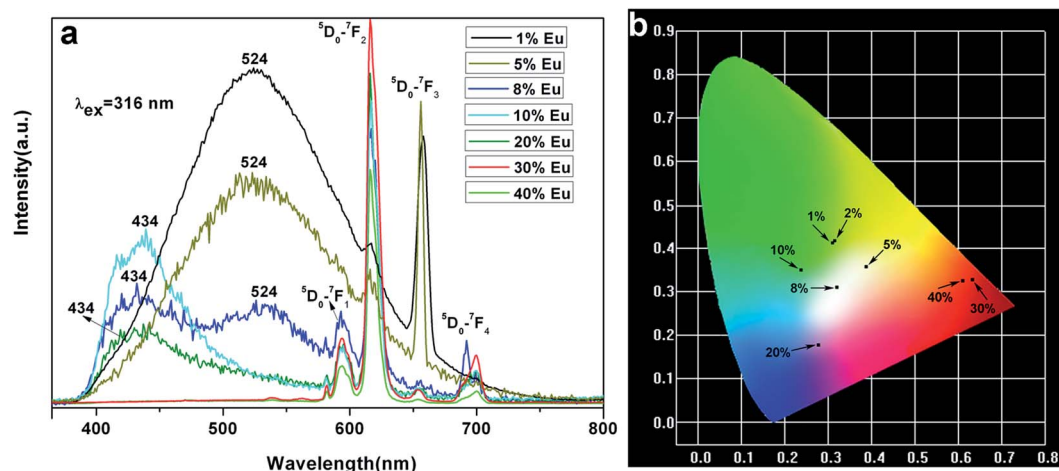
Fig. 7   (a) Emission spectra of InVO$_4$ doped with different doping concentrations of Eu^{3+}; (b) CIE chromaticity diagram for InVO$_4$ doped with different doping concentrations of Eu^{3+}.

because the much larger ions of Eu^{3+} occupied some of the crystal lattices instead of the smaller In^{3+} ions. And in the $InVO_4$:10% Eu^{3+} emission, the $InVO_4$ emission blue shifted to 434 nm completely, while the emission of Eu^{3+} gradually enhanced and dominated the emission spectrum instead of $InVO_4$. Then the emission of $InVO_4$ disappeared gradually with Eu^{3+} ion doping concentration increasing. The emission intensity of Eu^{3+} reached the maximum at 30% doping concentration. The concentration quenching effect occurs at Eu^{3+} concentrations higher than 30%, which is caused by the effect of energy exchange between Eu^{3+} ions as the distance between them decreases with increasing Eu^{3+} ion concentrations. The luminescence quantum efficiency (Φ) which fundamentally determined the luminescence properties of the materials was studied. The experimental value (Φ) of the $InVO_4$: 10% Eu^{3+} is 3.04%, while the value (Φ) of $InVO_4$: 30% Eu^{3+} is 15.38% with the same experimental conditions. It can be seen that the luminescence increased about 5 times when Eu^{3+} doping concentration increased from 10% to 30%.

It is interesting to find that the emission wavelength of $InVO_4$:5% Eu^{3+} and $InVO_4$:8% Eu^{3+} almost covers the whole visible region. The CIE chromaticity coordinates are $x = 3937$ $y = 3593$ for $InVO_4$:5% Eu^{3+} and $x = 0.3195$ $y = 0.3181$ for $InVO_4$:8% Eu^{3+} as shown in Fig. 7b, which could make these materials suitable candidates for white LEDs. Fig. 7b shows the CIE chromaticity diagram for $InVO_4$:Eu^{3+} phosphors. The CIE chromaticity coordinates of $InVO_4$:$x$$Eu^{3+}$ have been clearly marked with black spots in Fig. 7b corresponding to the emission of $InVO_4$:$x$$Eu^{3+}$ (x = 1–40%) shown in Fig. 7a. The emission colors are green, blue green, white and red for different Eu^{3+} ion concentrations. In this case, we can modulate the emission color region through $InVO_4$ doping with different concentrations of Eu^{3+}, which made the nanomaterials of $InVO_4$:Eu% excellent new materials for optoelectronic applications.

4 Conclusion

Uniform nanostructures of $InVO_4$:$x$$Eu^{3+}$ were obtained in this work. The $InVO_4$:$x$$Eu^{3+}$ products are different sizes of nanoparticles when the Eu^{3+} concentrations range from 0 mol% to 30 mol%, and middle-concave nanodisks or nanoparticles with different sizes when the Eu^{3+} concentrations range from 35 mol% to 45 mol%. The morphology difference is related to the large difference in ion radius between In^{3+} ions and Eu^{3+} ions. Emission colors of $InVO_4$:$x$$Eu^{3+}$ including green, blue-green, white and red light were obtained by modulating the Eu^{3+} ion doping concentration. When the Eu^{3+} doping concentration is less than 20%, the emissions originate both from Eu^{3+} and VO_4^{3-}, of which the emission of the $InVO_4$:5% Eu^{3+} and $InVO_4$:8% Eu^{3+} almost cover the whole visible region and exhibit white light. The emission intensity of Eu^{3+} ions reached a maximum at 30% doping concentration and $InVO_4$:30% Eu^{3+} also has the smallest size in morphology, which can be attributed to the quantum confinement effect of

the matrix where the Eu^{3+} ions were trapped. Research about micro/nanostructures of indium compounds is still in progress in our lab.

Conflicts of interest

There are no conflicts to declare.

Acknowledgements

References

1 (a) Z. L. Wang, *Mrs Bull.*, 2012, **37**, 814–827; (b) C. W. Cheng and H. J. Fan, *Nano Today*, 2012, **7**, 327–343.

2 (a) J. Ge, J. D. Lei and R. N. Zare, *Nat. Nanotechnol.*, 2012, **7**, 428–432; (b) D. Kowalski, D. Kim and P. Schmuki, *Nano Today*, 2013, **8**, 235–264.

3 J. H. Ye, Z. G. Zou, M. Oshikiri, A. Matsushita, M. Shimoda, M. Imai and T. Shishido, *Chem. Phys. Lett.*, 2002, **356**, 221–226.

4 J. C. Shen, H. Yang, Q. H. Shen and Z. Y. You, *Procedia Eng.*, 2014, **94**, 64–70.

5 Y.-S. Chang, Z.-R. Shi, Y.-Y. Tsai, S. Wu and H.-L. Chen, *Opt. Mater.*, 2011, **33**, 375–380.

6 Z. H. Ai, L. Z. Zhang and S. C. Lee, *J. Phys. Chem. C*, 2010, **114**, 18594–18600.

7 (a) J.-M. Yao, C.-K. Lee, S.-J. Yang and C.-S. Hwang, *J. Alloys Compd.*, 2009, **481**, 740–745; (b) T. H. Noh, D. W. Kim, S. W. Seo, I. S. Cho, D. H. Kim, H. S. Han and K. S. Hong, *Mater. Lett.*, 2012, **72**, 98–100; (c) L. W. Zhang, H. B. Fu, C. Zhang and Y. F. Zhu, *J. Solid State Chem.*, 2006, **179**, 804–811.

8 X. M. Liu, Y. Lu, C. Chen, S. L. Luo, Y. H. Zeng, X. Q. Zhang, M. M. Shang, C. X. Li and J. Lin, *J. Phys. Chem. C*, 2014, **118**, 27516–27524.

9 (a) K. Li, S. S. Liang, M. M. Shang, H. Z. Lian and J. Lin, *Inorg. Chem.*, 2016, **55**, 7593–7604; (b) K. Li, M. M. Shang, Y. Zhang, J. Fan, H. Z. Lian and J. Lin, *J. Mater. Chem. C*, 2015, **3**, 7096–7104.

10 R. D. Shannon, *Acta Crystallogr. A*, 1976, **32**, 751–767.

11 (a) H. W. Zhang, X. Y. Fu, S. Y. Niu, G. Q. Sun and Q. Xin, *Solid State Commun.*, 2004, **132**, 527–531; (b) Y. S. Chang, F. M. Huang, Y. Y. Tsai and L. G. Teoh, *J. Lumin.*, 2009, **129**, 1181–1185.

12 X. Wang and Y. D. Li, *Angew. Chem., Int. Ed.*, 2002, **41**, 4790–4793.

13 (a) H.-R. Shih, K.-T. Liu, L.-G. Teoh, L.-K. Wei and Y.-S. Chang, *Microelectron. Eng.*, 2015, **148**, 10–13; (b) Y. Luo, Z. G. Xia, B. F. Lei and Y. G. Liu, *RSC Adv.*, 2013, **3**, 22206–22212.